Author Manuscript

Author Manuscript

Author Manuscript

Author Manuscript

HHS Public Access

Author manuscript

J Biomed Mater Res A. Author manuscript; available in PMC 2021 May 01.

Published in final edited form as:

J Biomed Mater Res A. 2021 May ; 109(5): 733–744. doi:10.1002/jbm.a.37058.

A multilayered scaffold for regeneration of smooth muscle and connective tissue layers

Carly M. Garrison[1], **Anya Singh-Varma**[1], **Alexandra K. Pastino**[2], **Joseph A. M. Steele**[2], **Joachim Kohn**[2], **N. Sanjeeva Murthy**[2], **Jean E. Schwarzbauer**[1]

[1]Department of Molecular Biology, Princeton University, Princeton, New Jersey

[2]New Jersey Center for Biomaterials, Rutgers, The State University of New Jersey, Piscataway, New Jersey

Abstract

Tissue regeneration often requires recruitment of different cell types and rebuilding of two or more tissue layers to restore function. Here, we describe the creation of a novel multilayered scaffold with distinct fiber organizations—aligned to unaligned and dense to porous—to template common architectures found in adjacent tissue layers. Electrospun scaffolds were fabricated using a biodegradable, tyrosine-derived terpolymer, yielding densely-packed, aligned fibers that transition into randomly-oriented fibers of increasing diameter and porosity. We demonstrate that differently-oriented scaffold fibers direct cell and extracellular matrix (ECM) organization, and that scaffold fibers and ECM protein networks are maintained after decellularization. Smooth muscle and connective tissue layers are frequently adjacent in vivo; we show that within a single scaffold, the architecture supports alignment of contractile smooth muscle cells and deposition by fibroblasts of a meshwork of ECM fibrils. We rolled a flat scaffold into a tubular construct and, after culture, showed cell viability, orientation, and tissue-specific protein expression in the tube were similar to the flat-sheet scaffold. This scaffold design not only has translational potential for reparation of flat and tubular tissue layers but can also be customized for alternative applications by introducing two or more cell types in different combinations.

Keywords

complex tissue regeneration; extracellular matrix (ECM); multilayered electrospun scaffolds; synthetic polymer; tubular scaffold

1 | INTRODUCTION

A central goal of tissue engineering is the development of tailored bio-materials to promote the regeneration of a damaged tissue or organ. Often the damage involves two or more

Correspondence Jean E. Schwarzbauer, Department of Molecular Biology, Princeton University, Princeton, NJ 08540., jschwarz@princeton.edu.

CONFLICTS OF INTEREST

The authors declare no conflicts of interest.

SUPPORTING INFORMATION

Additional supporting information may be found online in the Supporting Information section at the end of this article.

Author Manuscript Author Manuscript Author Manuscript Author Manuscript

adjacent tissue layers, each with disparate cellular organizations and molecular compositions that are related to their specialized functions. For example, in many organs and tube-shaped tissues, a smooth muscle layer, essential for oriented tissue contraction and elasticity, is supported by a connective tissue meshwork of extracellular matrix (ECM) and fibroblasts.[1,2] A biomaterial that can provide regional cues to control the geometry and phenotype of cells, like smooth muscle cells (SMCs) and fibroblasts, in distinct locations would be greatly beneficial for regeneration of multiple tissue layers.

Electrospun scaffolds are highly utilized in tissue engineering applications.[3,4] Fiber architecture and mechanical properties can be tuned to yield structures that vary in porosity and alignment to resemble various types of tissue ECM organization.[5] Scaffolds can also be used in combination with bioactive cues, such as growth factors, ECM proteins, or cell-signaling peptides, to promote specific cell behaviors.[6–8] For an electrospun scaffold to support regeneration of adjacent tissue layers, its three-dimensional (3D) structure would need varying fiber architectures to template the different cell and ECM organizations in each layer as well as region-specific signals to induce appropriate cell phenotypes. Layered and graded formats of electrospun scaffolds have been reported that vary in mechanical properties, bioactivity, or fiber organization.[9–11] For example, tri-laminar composite scaffolds that mimic the properties and biochemical composition of cartilage have been fabricated.[12,13] Scaffolds that vary in porosity to allow cell infiltration or fluid flow have been described such as mixed electrospinning with a sacrificial polymer.[7,9] However, few reports describe scaffolds that vary in both fiber organization and density together.

In this study, we used sequential electrospinning to fabricate multilayered scaffolds with distinct fiber organizations, aligned/unaligned and dense/porous, generated by electrospinning of E1001(1k), a biodegradable tyrosine-derived terpolymer. E1001(1k) has been used for regeneration in nerve, bone, and other cellular environments, demonstrating its compatibility for growth of different cell types including osteoclasts and pre-osteoblasts.[14,15] Importantly, the polymer is degradable over a time period of 8 months, unlike ~3 years for the widely used polycaprolactone (PCL); and the degradable products are not acidic and thus are not inflammatory, unlike the widely used polylactic acid polymer.[16,17] Furthermore, E1001(1k) can be chemically tuned to customize the degradation profile and mechanical properties of a scaffold for a specific regenerative application.[18] The scaffold described here varies in fiber alignment and density. We demonstrate the ability of the aligned side of the scaffold in combination with the cytokine transforming growth factor-beta 1 (TGF-β1) to direct the alignment of contractile SMCs while fibroblasts simultaneously deposit a meshwork ECM supported by the unaligned side of the scaffold, thus recreating two neighboring tissue layers that are commonly found together in vivo. We show that the multilayered scaffold with SMCs and fibroblasts can be rolled and then cultured as a tube-shaped biomaterial, resembling the organization of smooth muscle and connective tissue in the walls of tubular tissues. In addition to smooth muscle/fibroblast layers, this multilayered scaffold should be applicable to other tissue layers by varying scaffold architecture or populating with different cell types.

Author Manuscript Author Manuscript Author Manuscript Author Manuscript

2 | MATERIALS AND METHODS

2.1 | Preparation of a multilayered electrospun scaffold

Scaffolds were prepared from the random block copolymer poly(DTE-*co*-10% DT-*co*-1% PEG carbonate) composed of desaminotyrosyl-tyrosine ethyl ester (DTE), desaminotyrosyl-tyrosine (DT), and PEG, that will be referred to as E1001(1k), where 10 and 01 are the mole percent of DT and PEG, respectively, and 1k is the molecular weight of PEG (1,000 Da).[16,18] The three components of the polymer serve different purposes. The main chain of DTE segments aids in polymer processing, has the required mechanical properties, and provides chemical stability during processing and use. Increasing the fraction of DT units increases the degradation rate from days at 25 mol % DT to hours at 50 mol % DT. Thus, 10 mol % DT used here provides a degradation rate of approximately 1 year. Because both DTE and DT are very hydrophobic, PEG was incorporated to increase water content and allow for degradation. PEG(1k) remains biocompatible after degradation and, unlike PEG(2k), does not crystallize in the scaffold.[19] The polymer was dissolved in hexafluoropropylene to prepare two solutions with concentration 16 and 10% that were used in electrospinning. The electrospinning apparatus consisted of a syringe pump (kd Scientific, Model 780100, Holliston, MA), high voltage DC power supply (Gamma High Voltage Research, Model ES30P/5W/DAM, Ormand Beach, FL) fitted with an 18 G needle, and a rotating mandrel. The syringe was placed 10 cm away from the mandrel. By laterally oscillating the 5 cm diameter mandrel, we obtained 13 × 21 cm fiber sheets. The speed of the mandrel was controlled by a DC power supply (Model 1627A, BK Precision, Yorba Linda, CA). The linear speed was set at 30 meters per minute (mpm) for unaligned layers and to 650 mpm for aligned layers. Multilayered scaffolds were prepared in three steps: 16% polymer solution was spun into an unaligned layer at 2 mL/hr for 30 min, followed by an additional unaligned layer with 10% solution at 1 mL/hr for 30 min, and finally an aligned layer with 10% solution at 1 mL/hr for 30 min. Fiber morphology was assessed using a scanning electron microscope (SEM) (Phenom ProX, Nanoscience Instruments, Phoenix, AZ) as well as a Nikon A1 confocal microscope in reflectance mode. NIS Elements-C software was used to create maximum intensity projections and volume reconstructions. The tyrosine-derived polymer scaffolds were autoflourescent across a range of wavelengths (400–800 nm). Scaffold thickness was measured using a micrometer as well as transverse SEM images and found to be 40–50 μm.

Scaffolds were electrospun as flat sheets and cut into 10 mm squares for culture. Cut scaffolds were secured to the bottom of a cell culture well with vacuum grease. For some experiments, 13 mm diameter and 160 μm tall PCL rings were 3D printed onto the electrospun scaffold to provide support and facilitate handling. For the transwell format, 14 mm tall PCL rings were printed onto the scaffold. Scaffolds with PCL rings were secured in the cell culture well by placing a plastic O-ring on top and sterilized by exposure to UV light for 1–2 hr.

2.2 | Cell culture and decellularization on E1001 (1k) scaffolds

NIH 3T3 cells (ATCC, Manassas, VA) and WKY3M22 rat SMCs (a gift from Victor Koteliansky)[20] were cultured in Dulbecco's modified Eagle's media (DMEM) containing 10

Author Manuscript Author Manuscript Author Manuscript Author Manuscript

or 5% bovine calf serum (BCS) (HyClone Laboratories, Logan, UT), respectively, and an antibiotic/antimycotic cocktail (Corning Life Sciences, Oneonta, NY) in a humidified CO_2 incubator at 37°C. Human fibroblast cells (BJ, ATCC CRL-2522) were grown in DMEM containing 10% fetal bovine serum (HyClone Laboratories). Then, 7.5×10^4 (4×10^4 cells/cm^2) fibroblasts or SMCs were seeded on the unaligned or aligned side of E1001 (1k) scaffolds and grown for 7 days, with media changed on Day 4. Recombinant human TGF-β1 protein was solubilized in 4 mM HCL, 0.1% BSA according to the manufacturer's instructions (R&D Systems, Minneapolis, MN, USA). For treatment of cells, 1×10^5 (5.3×10^4 cells/cm^2) SMCs or fibroblasts were grown for 2 days to confluence, after which medium was replaced with medium containing 2 ng/ml recombinant TGF-β1 protein or an equivalent volume of vehicle and cells were grown for an additional 3 days. For delivery of TGF-β1 by agarose droplet, a 1% low-melting point agarose (Sigma-Aldrich) solution was prepared in DMEM containing 5% BCS and 2 ng total of TGF-β1. Agarose droplets were placed on the unaligned side of the scaffold and solidified by incubating for 5 min at 4°C before cell seeding.

For decellularization, the standard Schwarzbauer lab protocol was used with the following modifications: an additional 15-min lysis buffer incubation, extension of the third lysis buffer incubation to 1.25 hr, and treatment with 20 U/ml DNase I (New England Biolabs Inc., Ipswich, MA) to remove any remaining nuclear material.[21]

2.3 | Fibrin-FN matrix contraction assay

Fibrin-FN matrices were prepared as described previously.[22,23] No additional FN or Factor XIII was required for clot formation. Cells were cultured for 24 hr in medium with 2 ng/ml TGF-β1 or vehicle before addition to clot components. Clots were carefully detached from the well walls using a thin needle under a dissecting microscope. The diameter of the clot was measured over 4 hr as described previously.[22,23] The percent contraction was averaged from nine total reactions from five independent experiments and normalized to the average contraction of a FN-fibrin clot that did not contain cells. Statistics were performed on contraction measurements and p-values were determined using the student's *t* test. *p*-Values less than .05 were considered to be significant.

2.4 | Tubular E1001(1k) scaffold construction

A 35 mm × 20 mm rectangle was cut from the scaffold sheet with fibers perpendicular to the long edge of the scaffold sheet. The cut scaffold was placed in a 60 mm dish and secured with vacuum grease. Then, 4×10^4 cells/cm^2 WKY3M22 SMCs were seeded and allowed to attach overnight. The scaffold was then rolled into a tube shape with the aligned SMC side on the inside, secured at the ends with cylinders cut from Plastic Pipet Tips, and moved into a 10-cm dish. A flat sheet of the same size and seeded with the same number of cells as the tube was used as a control. Cells were cultured for 7 days. Plastic cylinders were gently removed using tweezers while the tube was in aqueous medium. Squares were cut from different locations across the tube structure for staining and flattened between two coverslips for imaging.

Author Manuscript Author Manuscript Author Manuscript Author Manuscript

2.5 | Coculture of SMCs and fibroblasts

For flat scaffold coculture, a PCL-ringed scaffold was placed with the unaligned side up in a 24-well dish. NIH 3T3 fibroblasts were seeded on the top unaligned side in 200 μl of medium and allowed to attach for 3 hr. Unattached cells were removed by washing and the ringed scaffold was moved to a new well, inverted with the aligned side up, and secured between two plastic O-rings so that both sides of the scaffold were exposed to medium. WKY3M22 SMCs were seeded on the top aligned side and allowed to attach for 1 hr. The scaffold with cells and O-rings was transferred to a new well, cultured in NIH 3T3 cell medium for 2 days and then treated with 2 ng/ml recombinant human TGF-β1 protein as described above. Low seeding volumes, movement of the scaffold to new wells after seeding, and using O-rings to secure the scaffolds helped to segregate the cells on opposite sides of the scaffold. For tube coculture experiments, a scaffold sheet was cut as described above and 4×10^4 cells/cm^2 WKY3M22 SMCs were seeded onto the aligned side of the sheet scaffold. The next day, 4×10^4 cells/cm^2 NIH 3T3 fibroblasts were seeded onto the unaligned side. The coculture was incubated in fresh medium overnight and then rolled into a tube the next day. Cells in tubes were cultured in medium containing 2 ng/ml TGF-β1.

2.6 | Antibodies

The following primary antibodies were used for immunofluorescence: rabbit anti-fibronectin polyclonal antiserum (R457) diluted 1:50,[24] anti-human fibronectin monoclonal antibody culture supernatant (HFN7.1) diluted 1:300 (DSHB), and anti-alpha smooth muscle actin (α-SMA) monoclonal antibody clone 1A4 diluted 1:100 (ThermoFisher, 14-9760-82). Secondary antibodies were Alexa Fluor 568-goat anti-mouse IgG (H + L), Alexa Fluor 488-goat anti-rabbit IgG (H + L), and Alexa Fluor 568-goat anti-rabbit IgG (H + L) (Life Technologies, Grand Island, NY) all diluted 1:400. DAPI was diluted 1:400 (Sigma-Aldrich), and Texas Red-X Phalloidin diluted 1:50 (ThermoFisher, T7471). The following antibody dilutions were used for immunoblotting: 1A4 at 1:7,500, HFN7.1 at 1:2,000, anti-calponin at 1:1,000 (Sigma-Aldrich, C2687), rat-specific fibronectin monoclonal antibody IC3 at 1:2,000,[25,26] and GAPDH rabbit monoclonal antibody at 1:10,000 (Cell Signaling, 2118S). The secondary antibodies were either horseradish peroxidase-conjugated goat anti-rabbit IgG or goat anti-mouse IgG diluted 1:10,000 (Pierce Chemical Co., Rockford, IL).

2.7 | Immunofluorescence and microscopy

Samples were fixed with 3.7% paraformaldehyde (Sigma-Aldrich) in PBS for 15 min at room temperature. For some experiments, cells were permeabilized with 0.5% Triton X-100 (Sigma) in PBS for 15 min at room temperature. Scaffolds were stained with TrueBlack Lipofuscin Autofluorescence Quencher (Biotium, Fremont, CA) in 70% ethanol for 2 min at room temperature and blocked with 5% goat serum for either 30 min or overnight at 37 and 4°C, respectively. Incubations were at room temperature for 1 hr and dilutions were made in 2% ovalbumin in PBS. Samples were mounted using ProLong Gold anti-fade reagent (Life Technologies). Images were captured with a Nikon A1 confocal microscope in both fluorescence and reflectance mode. Images were reconstructed and analyzed using Nikon Elements and ImageJ software. To quantify immunofluorescence intensity of cells expressing α-SMA and actin, mean fluorescence intensity was measured and averaged for

Author Manuscript Author Manuscript Author Manuscript Author Manuscript

6–8 images per condition using FIJI Software (NIH, https://imagej.nih.gov). All fluorescence intensity quantification was performed on unadjusted 8-bit gray scale images. Images were adjusted for brightness and contrast for publication using FIJI; images compared to one another were adjusted equivalently.

FN matrix orientation was quantified by fast Fourier transform (FFT) analysis using five cropped (1,024 × 1,024) 8-bit images (×20 magnification). A gray scale mask was constructed as described previously using a gradation of gray scale pixels to account for edge artifacts.[27,28] Oval Profile Plugin (authored by William O'Connell) was used to determine the summed pixel intensity for each angle between 0 and 360°. Since the plot is nearly symmetrical, the radial intensity data were averaged and plotted from 0 to 180°, normalized to a baseline value of 0 and plotted in arbitrary units ranging from 0 to 0.10.

2.8 | Immunoblotting

Fibronectin was isolated from media by gelatin-Sepharose affinity chromatography (Sigma-Aldrich). To analyze intracellular proteins, cells were lysed with radioimmune precipitation buffer (1% NP-40, 0.5% Na-DOC, 0.1% SDS, 2 mM EDTA, 150 mM NaCl, 50 mM Tris–HCl, pH 7.4). Total protein quantifications were determined with BCA Protein Assay (Pierce). Samples were prepared with equal protein concentrations, resolved by SDS-PAGE on either 8, 10, or 13% polyacrylamide gels, and transferred to nitrocellulose membranes. Calponin and α-SMA blots were blocked with 5% nonfat dry milk (Lab Scientific) or 5% BSA (Sigma), respectively, in TBST, pH 7.8, overnight at 4°C. Chemiluminescence was conducted using SuperPlus ECL reagents (ThermoFisher). Densitometry was performed on scanned films using FIJI. Only exposures yielding signals within the linear range for control samples were quantified. Immunoblots of lysates from three independently performed experiments were analyzed and quantified signals were averaged across experiments.

3 | RESULTS

3.1 | Fabrication of an electrospun scaffold with distinct fiber organizations

We created an electrospun scaffold made of the polymer E1001 (1k) in which the scaffold fibers transition through three layers from highly aligned to randomly oriented. The aligned side of the scaffold, which was electrospun with a 10% polymer solution, is more uniform with 0.5–1 μm diameter fibers separated by 5–10 μm gaps oriented in a similar direction to one another as shown by SEM (Figure 1a) and confocal microscopy (Figure S1a). The unaligned section of the scaffold was spun with 10 and 16% polymer solutions to generate thicker fiber diameters ranging from 2–4 μm. Fiber diameters are thinner for the internal fibers and thicken closer to the surface of the unaligned side (Figures 1b and S1a). The scaffolds used here have overall thicknesses of 40–50 μm, but thickness can be increased by adjusting the spin time. Due to the opacity and light scattering of the scaffold fibers, it is not possible to image through the entirety of the scaffold using confocal microscopy. However, we were able to clearly image 20–30 μm into the scaffold from each side and visualize the transition in fiber organization by imaging at different planes across the layers of the scaffold. Dense aligned fibers extend across at least the top 8 μm of the scaffold (Figure 1c (a,b)). In the middle of the scaffold 26 μm in from each side (Figure 1c (c,c′)), fiber density

Author Manuscript Author Manuscript Author Manuscript Author Manuscript

is maintained but fibers show less alignment. Imaging through the unaligned side, the fibers are both less aligned and less densely packed creating a porous, randomly oriented structure (Figure 1c (d,e)). Quantification of scaffold fiber alignment by FFT analysis of confocal slices at different depths across the scaffold confirms a transition from aligned to unaligned fibers (Figure S1b). Thus, the scaffold consists of fiber densities that progress from dense to porous and fiber orientations from aligned to unaligned.

3.2 | Cell and ECM organization in response to scaffold fiber orientations

To investigate the effect of the scaffold fiber orientation on cell and matrix fibril organization, we cultured mouse NIH 3T3 fibroblasts separately on aligned and unaligned sides of the electrospun scaffolds. The cells attached equivalently on the two sides of the scaffold and assembled a dense FN-rich matrix. We did not observe differences in fibroblast proliferation between the two scaffold sides; cells on aligned and unaligned scaffold sides reached confluence at the same time (data not shown). On the aligned side, cells were oriented with the scaffold fibers (Figure S2) and assembled FN fibrils parallel to the scaffold fibers (Figure 2a). On the unaligned side, cells were in various orientations (Figure S2) and the cell-assembled matrix was a meshwork array of fibrils (Figure 2b). The degree of matrix alignment for each side of the scaffold was quantified using FFT analysis. The radial summation of pixel intensity data for each angle is plotted from 0 to 180° with the peak at 90° indicating global parallel alignment of FN fibrils across the aligned scaffold surface (Figure 2c). The lack of an obvious peak for FN matrix on the unaligned side indicates the lack of a preferred orientation for FN fibrils. A major concern for the use of electrospun scaffolds in tissue regeneration is lack of cell infiltration into scaffolds in order to create a 3D cell-scaffold construct.[29] Infiltration into the aligned side of the scaffold was limited; cells and matrix were confined to the top of the scaffold whereas cells infiltrated the unaligned side of the multilayered scaffold and nuclei could be detected at least 20 μm deep (Figure S3). Thus, our multilayered scaffold supports unidirectional cell infiltration so that cells on one side are confined to a monolayer organization while cells on the other side have a 3D organization embedded in their ECM.

To test the stability of both the scaffold fibers and ECM, we analyzed their organizations after a decellularization procedure.[7,21] Imaging revealed a dense meshwork of matrix fibrils on top and within the scaffold after cell removal and the differing FN matrix organizations on either side of the scaffold were preserved (Figure S4). Importantly, the high pH of the decellularization solutions did not negatively affect the organization of the scaffold fibers. Thus, we can generate two differently oriented ECM-synthetic fiber structures within one scaffold by varying the scaffold fiber properties to direct distinct cell and ECM organizations.

3.3 | Scaffold permeability

Cells infiltrate the porous unaligned scaffold but are unable to move through the aligned fibers, indicating that cells from opposite sides of the scaffold do not directly interact. However, they may still communicate through the exchange of secreted proteins. To test permeability, scaffolds were fabricated with a 3D-printed ring in a transwell format, a design that allows access of media to each side of the scaffold while maintaining separate inside

Author Manuscript Author Manuscript Author Manuscript Author Manuscript

and outside compartments (Figure 3a). PBS added to the inside of the transwell freely passed through to the other side of the scaffold. The transit of serum proteins through a transwell scaffold with a confluent, aligned SMC layer was monitored over 24 hr. Serum albumin at 67 kDa and other serum proteins were detected at the earliest timepoint of 30 min and serum protein levels equilibrated between the two compartments by 8 hr (Figure 3b). SMCs secrete FN, a much larger 500 kDa protein, and our analysis also showed that FN traversed the cell-scaffold thickness (Figure 3c). These results show that proteins freely diffuse across a multilayered scaffold populated with cells.

3.4 | Directing SMC phenotype on an aligned scaffold

SMCs have the ability to undergo phenotypic switching between a “contractile” phenotype, characterized by an increase in myofilaments and expression of contractile proteins, such as α-SMA, calponin, and h-caldesmon, and a “synthetic” phenotype characterized by increased proliferation and ECM synthesis and a decrease in contractile protein markers.[30–32] Healthy, adult smooth muscle tissue primarily consists of contractile SMCs that are aligned to provide an oriented contractile force.[33] Topographical cues can stimulate both SMC alignment and increased expression of contractile protein markers.[34–36] Aberrant switching of SMC phenotype from contractile to synthetic is thought to underlie the development of disease, making it crucial to control SMC phenotype in an implanted scaffold.[37–39] When SMCs were cultured on the aligned side of the multilayered scaffold, they grew to confluence and aligned with scaffold fibers. Only a small percentage of cells had stress fibers containing α-SMA (Figure 4a) suggesting that SMC alignment on the scaffold fibers was not sufficient to promote a contractile phenotype.

The cytokine TGF-β1 can promote a contractile phenotype[40–42] and we found that treatment of SMCs on an aligned scaffold with TGF-β1 increased the number of α-SMA stress fibers and the mean fluorescence intensity by 2.1 ± 0.6-fold ($p < .001$) compared to control, while the mean fluorescence intensity of total actin stress fibers was unchanged (1.0 ± 0.2-fold, $p = .42$) (Figure 4a). Additionally, TGF-β1 treatment increased expression of the contractile protein markers α-SMA (4.0 ± 0.9-fold) and calponin (1.9 ± 0.2-fold) (Figure 4b). To directly test whether the increased contractile protein expression stimulated SMC contractility, we performed a matrix contraction assay using SMCs treated with either TGF-β1 or vehicle control in a 3D fibrin-FN matrix.[22,23] Contraction by TGF-β1-treated SMCs was significantly greater than by control SMCs (27.2% ± 2.2 vs. 16.4% ± 1.5) (Figure 4c). We conclude that while the aligned fibers of the scaffold direct SMCs into an aligned cell layer, addition of TGF-β1 is required to enhance the contractile phenotype.

To determine whether we can incorporate cell differentiation cues into the multilayered scaffold, a drop of low-melting point agarose with or without TGF-β1 was deposited within the unaligned fibers of the scaffold and SMCs were cultured on the opposite aligned side. Differentiation was monitored by staining for assembly of α-SMA. Our results show that, compared to control, the TGF-β1 droplet stimulated a significant increase in α-SMA stress fibers similar to the level observed with global delivery of TGF-β1 (Figure S5). Thus, localized delivery of TGF-β1 promotes a contractile SMC.

Author Manuscript Author Manuscript Author Manuscript Author Manuscript

3.5 | Communication between smooth muscle and connective tissue layers in a scaffold

In vivo, proteins diffuse through tissues and across tissue layers to affect cell functions in other compartments. For example, FN circulating in blood plasma crosses the endothelium to become incorporated into the underlying ECM of most tissues and organs.[43–45] To test if FN matrix assembly occurs across layers in the scaffold, we cultured human fibroblasts on the unaligned outside and rat SMCs on the aligned inside of a transwell scaffold. Immunoblotting of FN from the medium on each side of the transwell with species-specific antibodies detected human FN and rat FN in both compartments (Figure 5a), showing diffusion across the cell-scaffold material. Immunofluorescence analyses with an anti-human FN specific antibody showed that not only did human fibroblasts on the outside of the transwell scaffold produce and assemble a dense FN matrix, but human FN was also incorporated into the matrix assembled by rat SMCs on the inside of the transwell (Figure 5b). Therefore, FN can travel through the scaffold between the cell layers and contribute to matrices at a distance, similar to what occurs in vivo.

FN has been shown to promote a synthetic SMC phenotype[46] raising the possibility that SMC assembly of FN produced by nearby fibroblasts might have an impact on SMC phenotype. Thus, we wondered if TGF-β1 treatment could still induce a contractile phenotype when SMCs and fibroblasts were cocultured in the scaffold. NIH 3T3 cells growing on the unaligned side and SMCs on the aligned side of the scaffold were treated with TGF-β1 and then stained for FN and α-SMA. Both cell types reached confluence on their respective scaffold sides. SMCs and their FN fibrils were aligned in a similar direction whereas the NIH 3T3 cells were not aligned and had a meshwork FN organization (Figure 6). SMCs with α-SMA stress fibers in this coculture were comparable to SMCs cultured alone on the scaffold. Importantly, the NIH 3T3 cells did not develop α-SMA stress fibers (Figure 6). SMCs had a higher α-SMA mean fluorescence intensity of 1.37 compared to the NIH 3T3 cell layer. This difference in intensity combined with visible α-SMA stress fibers in SMCs but not fibroblasts shows that we can use the multilayered scaffold in conjunction with TGF-β1 to control both the organization and phenotype of two separate cell layers in order to maintain an aligned, contractile SMC layer while also supporting a porous FN-rich fibroblast layer.

3.6 | Converting a flat scaffold into a tube

Many tubular tissues have adjacent smooth muscle and connective tissue layers.[47] To determine if a cell-seeded scaffold could be translated into a tubular construct, SMCs were allowed to adhere to the aligned side of a rectangular scaffold sheet and then the scaffold was rolled into a tubular shape, with the scaffold fibers aligned circumferentially. To maintain the rolled shape, short plastic cylinders were used to secure the ends of the tube (Figure S6a) and tubes were then cultured for 1 week, sufficient time for cells to grow to confluence and assemble a FN matrix when in the flat scaffold format. The plastic cylinders were removed and, surprisingly, the scaffold retained a tubular shape without external support (Figure S6a). We speculate that the confluent, aligned SMC layer with its supporting ECM reinforced the mechanical stability of the tube and allowed for shape retention after removal of the plastic cylinders. Because of the flexibility of the synthetic material, we could roll a cell-seeded scaffold into a tube for cell culture but then unroll it after culture to

Author Manuscript Author Manuscript Author Manuscript Author Manuscript

analyze cell proliferation and matrix assembly. Analysis of cell viability and orientation within the tube by actin staining demonstrated the cells had grown to confluence and were aligned with the scaffold fibers (Figures 7a and S6b), similarly to cells grown on a flat scaffold. We were also able to directly electrospin a multilayered scaffold in a sealed, tubular format (Figure S7). To generate a tube with two tissue layers, a scaffold with SMCs attached to the aligned side and fibroblasts to the unaligned side was rolled with the aligned side in and then cultured with TGF-β1. Cells reached confluence on both sides of the scaffold and showed the expected organization of fibroblasts within a meshwork array of FN fibrils and of SMCs aligned with their matrix (Figure 7b). α-SMA stress fibers were evident in the SMCs but less so in the NIH 3T3 cells, with SMCs having a mean fluorescence intensity of 1.42 compared to the fibroblasts. This strategy has the advantage that cells are grown on the flat scaffold, which promotes uniform cell seeding, uniform delivery of soluble factors and other cell treatments, and ease of analysis, prior to rolling into a tube for implant.

4 | DISCUSSION

During tissue regeneration and repair, multiple tissue layers with dis-similar structure and function need to be reestablished simultaneously. We created a novel, multilayered electrospun scaffold that transitions from a highly aligned, dense fiber network into a porous, unaligned structure, a common organization across neighboring tissue layers. The scaffold fiber density allows diffusion of proteins at least as large as fibronectin, thus permitting communication between cells on opposite sides through exchange of cell-specific factors. Using this scaffold design, we were able to simultaneously direct SMCs and fibroblasts to adopt aligned and unaligned cell and ECM organizations, respectively. Treatment of this coculture with TGF-β1 induced development of a contractile SMC phenotype without changing α-SMA expression by fibroblasts. Thus, this novel scaffold structure has the ability to recreate multiple tissue layers simultaneously, including treatment with a cell differentiation factor, in both flat and tubular formats, and can be utilized in combination with soluble factors or ECM proteins to promote cell-specific phenotypes found in adjacent tissue layers.

An important feature of this scaffold is that it supports unidirectional cell infiltration. Cells are confined to a monolayer on the aligned side of the scaffold where fibers are densely packed. In contrast, infiltration into the unaligned scaffold side allowed for a 3D organization of cells and ECM that resembles connective tissue in vivo. Cells primarily penetrated the scaffold layer spun with a 16% polymer solution, which generates thicker diameter fibers with larger pores. In contrast to the multilayered scaffold, when cells were analyzed on a bilayer scaffold consisting of aligned and unaligned layers, both spun with a 10% polymer solution, cell infiltration was significantly inhibited (CMG, unpublished observations). Fiber densities throughout the multilayered scaffold did not prevent protein diffusion through the structure. FN produced by cells on one side diffused to the other side where it could be incorporated into the matrix. Therefore, in addition to customizing the composition and orientation of cell-derived ECM by changing the cell types on either side of the scaffold, one could also supplement the matrix on one side with ECM proteins produced by cells on the other side. After implant, a scaffold customized with tissue-specific cells and their ECM could act as a template for infiltration of endogenous cell types, and because

Author Manuscript Author Manuscript Author Manuscript Author Manuscript

E1001(1k) is biodegradable, the gradual loss of fiber mass would allow cells to replace synthetic fibers with tissue-specific ECM. FN forms a foundational matrix that is required for the matrix deposition of many other ECM proteins including collagens.[48–50] We expect that the distributions and organizations of these other ECM proteins will follow FN fibrils in alignment or as a meshwork.

Others have utilized scaffold constructs to coculture relevant cell types found in adjacent tissues, such as endothelial cells, SMCs, and fibroblasts.[51,52] It has been reported that cell differentiation and certain cell phenotypes can be promoted in coculture compared to monoculture.[53,54] In contrast to our work, these studies did not direct adjacent cell layers to form distinct tissue architectures. In our study, the multilayered scaffold in combination with TGF-β1 promoted a contractile phenotype in SMCs on the aligned side of the scaffold without affecting the phenotype of fibroblasts cocultured on the opposite, unaligned side of the scaffold. This demonstrates the ability to utilize the multilayered scaffold in combination with external factors to manipulate the phenotype of one cell layer without significantly adversely affecting the phenotype of cells on the other side of the scaffold. While we focused solely on SMCs and fibroblasts, this scaffold is compatible with other cell types (CMG, unpublished observations) allowing for customization to specific tissue engineering efforts by varying cell layer pairings.

Significant progress has been made in the development of tube scaffolds for the replacement of tubular tissues, such as a blood vessel.[55–57] Many of these constructs require in vivo recellularization by host cells, but recently, there has been an increase in studies using in vitro cell seeding of tube scaffolds.[58,59] One significant advantage of our tube construct is that cells are seeded and grown on the flat scaffold prior to rolling into a tube, eliminating the challenge of obtaining evenly distributed cell adhesion and growth inside of the tube.[60] Indeed, some groups are addressing this problem by focusing on shape-changing polymers to form self-rolled tubes, where scaffolds can be populated with relevant cell types in 2D and then be induced to change shape after implantation in vivo.[61,62] A second advantage of the multilayered scaffold is that a single scaffold controls the cell and ECM organizations in separate but adjacent tissue layers. The tissue layers are determined by the types of cells seeded in the scaffold. Third, our system is easily combined with other biological factors for the promotion of specific phenotypes, which is a major benefit for cell types with the ability to differentiate or undergo phenotypic switching. Finally, E1001(1k) is a nontoxic, biodegradable material.[16,17] Thus, we anticipate that after implantation of a cell-seeded scaffold in vivo, cells on both sides of the scaffold as well as endogenous cells will be able to infiltrate further in as the scaffold degrades, replacing the degraded scaffold with ECM and new tissue. Previous studies have shown that when endothelial cells are seeded onto an SMC layer, they can attach, proliferate, and form a monolayer.[50] Thus, our coculture system could be adapted to add a third tissue layer consisting of endothelial cells, recapitulating the multiple cell layer structure of organs such as the esophagus, blood vessel, and urinary bladder.

Supplementary Material

Refer to Web version on PubMed Central for supplementary material.

Author Manuscript Author Manuscript Author Manuscript Author Manuscript

ACKNOWLEDGMENTS

The authors are grateful Dr. Gary Laevsky, director of the Molecular Biology Confocal Microscopy Core Facility, a Nikon Center of Excellence, for his technical assistance and members of the Schwarzbauer lab for insightful discussions. The authors also thank Dr. Victor Koteliansky for kindly supplying WKY3M22 SMCs. The authors gratefully acknowledge support for this research from the National Institutes of Health to RESBIO—The National Resource for Polymeric Biomaterials (P4 EB001046) (to J. K.) and R01 AR 073236 (to J. E. S.). C. M. G. was supported by the New Jersey Commission on Cancer Research (NJCCR) DFHS18PPC041 predoctoral fellowship and NIH T32 GM007388 predoctoral training grant to the Department of Molecular Biology at Princeton University.

Funding information

National Institute of Arthritis and Musculoskeletal and Skin Diseases, Grant/Award Number: R01 AR 073236; National Institute of Biomedical Imaging and Bioengineering, Grant/Award Number: P4 EB001046; National Institute of General Medical Sciences, Grant/Award Number: NIH T32 GM007388; New Jersey Commission on Cancer Research (NJCCR), Grant/Award Number: DFHS18PPC041

Abbreviations:

α-SMA	alpha smooth muscle actin
ECM	extracellular matrix
FFT	fast Fourier transform
FN	fibronectin
PCL	polycaprolactone
PEG	polyethylene glycol
SEM	scanning electron microscopy
SMC	smooth muscle cell
TGF-β1	transforming growth factor-beta 1

REFERENCES

1. Zderic SA, Chacko S. Alterations in the contractile phenotype of the bladder: lessons for understanding physiological and pathological remodeling of smooth muscle. J Cell Mol Med. 2012;16(2):203–217. [PubMed: 21707917]
2. Heidari M, Mandato CA, Lehoux S. Vascular smooth muscle cell phenotypic modulation and the extracellular matrix. Artery Res. 2019;9 (C):14–18.
3. Li WJ, Laurencin CT, Caterson EJ, Tuan RS, Ko FK. Electrospun nanofibrous structure: a novel scaffold for tissue engineering. J Biomed Mater Res. 2002;60(4):613–621. [PubMed: 11948520]
4. Ameer JM, Pr AK, Kasoju N. Strategies to tune electrospun scaffold porosity for effective cell response in tissue engineering. J Funct Biomater. 2019;10(3):30.
5. Sill TJ, von Recum HA. Electrospinning: applications in drug delivery and tissue engineering. Biomaterials. 2008;29(13):1989–2006. [PubMed: 18281090]
6. Ardila DC, Tamimi E, Doetschman T, Wagner WR, Vande Geest JP. Modulating smooth muscle cell response by the release of TGFβ2 from tubular scaffolds for vascular tissue engineering. J Control Release. 2019;299:44–52. [PubMed: 30797003]
7. Goyal R, Vega ME, Pastino AK, et al. Development of hybrid scaffolds with natural extracellular matrix deposited within synthetic polymeric fibers. J Biomed Mater Res A. 2017;105(8):2162–2170. [PubMed: 28371271]

Author Manuscript Author Manuscript Author Manuscript Author Manuscript

8. Gao X, Zhang X, Song J, et al. Osteoinductive peptide-functionalized nanofibers with highly ordered structure as biomimetic scaffolds for bone tissue engineering. Int J Nanomedicine. 2015;10:7109–7128. [PubMed: 26604759]
9. Kidoaki S, Kwon IK, Matsuda T. Mesoscopic spatial designs of nano-and microfiber meshes for tissue-engineering matrix and scaffold based on newly devised multilayering and mixing electrospinning techniques. Biomaterials. 2005;26(1):37–46. [PubMed: 15193879]
10. Mahjour SB, Sefat F, Polunin Y, Wang L, Wang H. Improved cell infiltration of electrospun nanofiber mats for layered tissue constructs. J Biomed Mater Res A. 2016;104(6):1479–1488. [PubMed: 26845076]
11. Scaffaro R, Lopresti F, Maio A, Sutera F, Botta L. Development of polymeric functionally graded scaffolds: a brief review. J Appl Biomater Funct Mater. 2017;15(2):e107–e121. [PubMed: 28009418]
12. McCullen SD, Autefage H, Callanan A, Gentleman E, Stevens MM. Anisotropic fibrous scaffolds for articular cartilage regeneration. Tissue Engineering. Part A. 2012;18(19–20):2073–2083. [PubMed: 22655795]
13. Steele JA, McCullen SD, Callanan A, et al. Combinatorial scaffold morphologies for zonal articular cartilage engineering. Acta Biomater. 2014;10(5):2065–2075. [PubMed: 24370641]
14. Kim J, Magno MH, Alvarez P, Darr A, Kohn J, Hollinger JO. Osteogenic differentiation of pre-osteoblasts on biomimetic tyrosine-derived polycarbonate scaffolds. Biomacromolecules. 2011;12(10): 3520–3527. [PubMed: 21834593]
15. Merolli A, Fung S, Murthy NS, et al. “Ruffled border” formation on a CaP-free substrate: A first step towards osteoclast-recruiting bone-grafts materials able to re-establish bone turn-over. J Mater Sci Mater Med. 2018;29(4):38. [PubMed: 29564568]
16. Magno MHR, Kim J, Srinivasan A, et al. Synthesis, degradation and biocompatibility of tyrosine-derived polycarbonate scaffolds. J Mater Chem. 2010;20:8885–8893.
17. Kim J, Magno MH, Ortiz O, et al. Next-generation resorbable polymer scaffolds with surface-precipitated calcium phosphate coatings. Regen Biomater. 2015;2(1):1–8. [PubMed: 26813289]
18. Yu C, Kohn J. Tyrosine-PEG-derived poly(ether carbonate)s as new biomaterials. Part I: synthesis and evaluation. Biomaterials. 1999;20 (3):253–264. [PubMed: 10030602]
19. Murthy NS, Wang W, Kohn J. Separation in copolymers of hydrophilic PEG blocks and hydrophobic tyrosine-derived segments using simultaneous SAXS/WAXS/DSC. Polymer. 2010;51:3978–3988. [PubMed: 20802835]
20. Graves DC, Yablonka-Reuveni Z. Vascular smooth muscle cells spontaneously adopt a skeletal muscle phenotype: a unique Myf5 (−)/MyoD(+) myogenic program. J Histochem Cytochem. 2000;48(9): 1173–1193. [PubMed: 10950875]
21. Harris GM, Raitman I, Schwarzbauer JE. Cell-derived decellularized extracellular matrices. Methods Cell Biol. 2018;143:97–114. [PubMed: 29310794]
22. Corbett SA, Schwarzbauer JE. Requirements for alpha(5)beta (1) integrin-mediated retraction of fibronectin-fibrin matrices. J Biol Chem. 1999;274(30):20943–20948. [PubMed: 10409640]
23. Midwood KS, Schwarzbauer JE. Tenascin-C modulates matrix contraction via focal adhesion kinase- and rho-mediated signaling pathways. Mol Biol Cell. 2002;13(10):3601–3613. [PubMed: 12388760]
24. Aguirre KM, McCormick RJ, Schwarzbauer JE. Fibronectin self-association is mediated by complementary sites within the amino-terminal one-third of the molecule. J Biol Chem. 1994;269(45):27863–27868. [PubMed: 7961716]
25. Sechler JL, Takada Y, Schwarzbauer JE. Altered rate of fibronectin matrix assembly by deletion of the first type III repeats. J Cell Biol. 1996;134(2):573–583. [PubMed: 8707839]
26. Sechler JL, Schwarzbauer JE. Coordinated regulation of fibronectin fibril assembly and actin stress fiber formation. Cell Adhes Commun. 1997;4(6):413–424. [PubMed: 9177903]
27. Ayres CE, Jha BS, Meredith H, et al. Measuring fiber alignment in electrospun scaffolds: a user’s guide to the 2D fast Fourier transform approach. J Biomater Sci Polym Ed. 2008;19(5):603–621. [PubMed: 18419940]

Author Manuscript Author Manuscript Author Manuscript Author Manuscript

28. Singh S, Bandini SB, Donnelly PE, Schwartz J, Schwarzbauer JE. A cell-assembled, spatially aligned extracellular matrix to promote directed tissue development. J Mater Chem B. 2014;2(11):1449–1453. [PubMed: 24707354]
29. Wu J, Hong Y. Enhancing cell infiltration of electrospun fibrous scaffolds in tissue regeneration. Bioact Mater. 2016;1(1):56–64. [PubMed: 29744395]
30. Ueki N, Sobue K, Kanda K, Hada T, Higashino K. Expression of high and low molecular weight caldesmons during phenotypic modulation of smooth muscle cells. Proc Natl Acad Sci U S A. 1987;84(24):9049–9053. [PubMed: 3321066]
31. Sobue K, Hayashi K, Nishida W. Expressional regulation of smooth muscle cell-specific genes in association with phenotypic modulation. Mol Cell Biochem. 1999;190(1–2):105–118. [PubMed: 10098977]
32. Rensen SS, Doevendans PA, van Eys GJ. Regulation and characteristics of vascular smooth muscle cell phenotypic diversity. Neth Heart J. 2007;15(3):100–108. [PubMed: 17612668]
33. Webb RC. Smooth muscle contraction and relaxation. Adv Physiol Educ. 2003;27(1–4):201–206. [PubMed: 14627618]
34. Shen JY, Chan-Park MB, He B, et al. Three-dimensional micro-channels in biodegradable polymeric films for control orientation and phenotype of vascular smooth muscle cells. Tissue Eng. 2006;12(8): 2229–2240. [PubMed: 16968163]
35. Agrawal A, Lee BH, Irvine SA, et al. Smooth muscle cell alignment and phenotype control by melt spun polycaprolactone fibers for seeding of tissue engineered blood vessels. Int J Biomater. 2015;2015: 434876. [PubMed: 26413093]
36. Han DG, Ahn CB, Lee J, et al. Optimization of electrospun poly(caprolactone) fiber diameter for vascular scaffolds to maximize smooth muscle cell infiltration and phenotype modulation. Polymers. 2019;11(4):693.
37. Katsuda S, Boyd HC, Fligner C, Ross R, Gown AM. Human atherosclerosis. III. Immunocytochemical analysis of the cell composition of lesions of young adults. Am J Pathol. 1992;140(4):907–914. [PubMed: 1562051]
38. Owens GK, Kumar MS, Wamhoff BR. Molecular regulation of vascular smooth muscle cell differentiation in development and disease. Physiol Rev. 2004;84(3):767–801. [PubMed: 15269336]
39. Wamhoff BR, Hoofnagle MH, Burns A, Sinha S, McDonald OG, Owens GK. A G/C element mediates repression of the SM22alpha promoter within phenotypically modulated smooth muscle cells in experimental atherosclerosis. Circ Res. 2004;95(10):981–988. [PubMed: 15486317]
40. Hautmann MB, Madsen CS, Owens GK. A transforming growth factor beta (TGFbeta) control element drives TGFbeta-induced stimulation of smooth muscle alpha-actin gene expression in concert with two CArG elements. J Biol Chem. 1997;272(16):10948–10956. [PubMed: 9099754]
41. Deaton RA, Su C, Valencia TG, Grant SR. Transforming growth factor-beta1-induced expression of smooth muscle marker genes involves activation of PKN and p38 MAPK. J Biol Chem. 2005;280(35):31172–31181. [PubMed: 15980430]
42. Beamish JA, He P, Kottke-Marchant K, Marchant RE. Molecular regulation of contractile smooth muscle cell phenotype: implications for vascular tissue engineering. Tissue Eng Part B Rev. 2010;16(5): 467–491. [PubMed: 20334504]
43. Oh E, Pierschbacher M, Ruoslahti E. Deposition of plasma fibronectin in tissues. Proc Natl Acad Sci U S A. 1981;78(5):3218–3221. [PubMed: 6789333]
44. Moretti FA, Chauhan AK, Iaconcig A, Porro F, Baralle FE, Muro AF. A major fraction of fibronectin present in the extracellular matrix of tissues is plasma-derived. J Biol Chem. 2007;282(38):28057–28062. [PubMed: 17644525]
45. Kumra H, Sabatier L, Hassan A, et al. Roles of fibronectin isoforms in neonatal vascular development and matrix integrity. PLoS Biol. 2018; 16(7):e2004812. [PubMed: 30036393]
46. Hedin U, Bottger BA, Forsberg E, Johansson S, Thyberg J. Diverse effects of fibronectin and laminin on phenotypic properties of cultured arterial smooth muscle cells. J Cell Biol. 1988;107(1):307–319. [PubMed: 2455726]
47. Jaslove JM, Nelson CM. Smooth muscle: a stiff sculptor of epithelial shapes. Philos Trans R Soc Lond B Biol Sci. 2018;373(1759):20170318. [PubMed: 30249770]

Author Manuscript Author Manuscript Author Manuscript Author Manuscript

48. Velling T, Risteli J, Wennerberg K, Mosher DF, Johansson S. Polymerization of type I and III collagens is dependent on fibronectin and enhanced by integrins alpha 11beta 1 and alpha 2beta 1. J Biol Chem. 2002;277(40):37377–37381. [PubMed: 12145303]

49. Kinsey R, Williamson MR, Chaudhry S, et al. Fibrillin-1 microfibril deposition is dependent on fibronectin assembly. J Cell Sci. 2008;121 (Pt 16):2696–2704. [PubMed: 18653538]

50. Miller CG, Pozzi A, Zent R, Schwarzbauer JE. Effects of high glucose on integrin activity and fibronectin matrix assembly by mesangial cells. Mol Biol Cell. 2014;25(16):2342–2350. [PubMed: 24943838]

51. Zhang X, Wang X, Keshav V, et al. Dynamic culture conditions to generate silk-based tissue-engineered vascular grafts. Biomaterials. 2009; 30(19):3213–3223. [PubMed: 19232717]

52. Ye L, Cao J, Chen L, et al. The fabrication of double layer tubular vascular tissue engineering scaffold via coaxial electrospinning and its 3D cell coculture. J Biomed Mater Res A. 2015;103(12):3863–3871. [PubMed: 26123627]

53. Hussain A, Collins G, Yip D, Cho CH. Functional 3-D cardiac co-culture model using bioactive chitosan nanofiber scaffolds. Biotechnol Bioeng. 2013;110(2):637–647. [PubMed: 22991229]

54. Lee B, Shafiq M, Jung Y, Park JC, Kim SH. Characterization and preparation of bio-tubular scaffolds for fabricating artificial vascular grafts by combining electrospinning and a co-culture system. Macromol Res. 2016;24:131–142.

55. Panseri S, Cunha C, Lowery J, et al. Electrospun micro- and nanofiber tubes for functional nervous regeneration in sciatic nerve transections. BMC Biotechnol. 2008;8:39. [PubMed: 18405347]

56. Evrova O, Houska J, Welti M, et al. Bioactive, elastic, and biodegradable emulsion electrospun DegraPol tube delivering PDGF-BB for tendon rupture repair. Macromol Biosci. 2016;16(7):1048–1063. [PubMed: 27071839]

57. Wu T, Zhang J, Wang Y, et al. Fabrication and preliminary study of a biomimetic tri-layer tubular graft based on fibers and fiber yarns for vascular tissue engineering. Mater Sci Eng C Mater Biol Appl. 2018;82: 121–129. [PubMed: 29025640]

58. Bye FJ, Bissoli J, Black JL, et al. Development of a bilayer and trilayer nanofibrous/microfibrous scaffolds for regenerative medicine. Biomater Sci. 2013;1:942–951. [PubMed: 32481963]

59. Wang Y, Shi H, Qiao J, et al. Electrospun tubular scaffold with circumferentially aligned nanofibers for regulating smooth muscle cell growth. ACS Appl Mater Interfaces. 2014;6(4):2958–2962. [PubMed: 24417638]

60. Villalona GA, Udelsman B, Duncan DR, et al. Cell-seeding techniques in vascular tissue engineering. Tissue Eng Part B Rev. 2010;16(3): 341–350. [PubMed: 20085439]

61. Zakharchenko S, Sperling E, Ionov L. Fully biodegradable self-rolled polymer tubes: a candidate for tissue engineering scaffolds. Biomacromolecules. 2011;12(6):2211–2215. [PubMed: 21524116]

62. Teshima TF, Nakashima H, Ueno Y, Sasaki S, Henderson CS, Tsukada S. Cell assembly in self-foldable multi-layered soft micro-rolls. Sci Rep. 2017;7(1):17376. [PubMed: 29273722]

Author Manuscript Author Manuscript Author Manuscript Author Manuscript

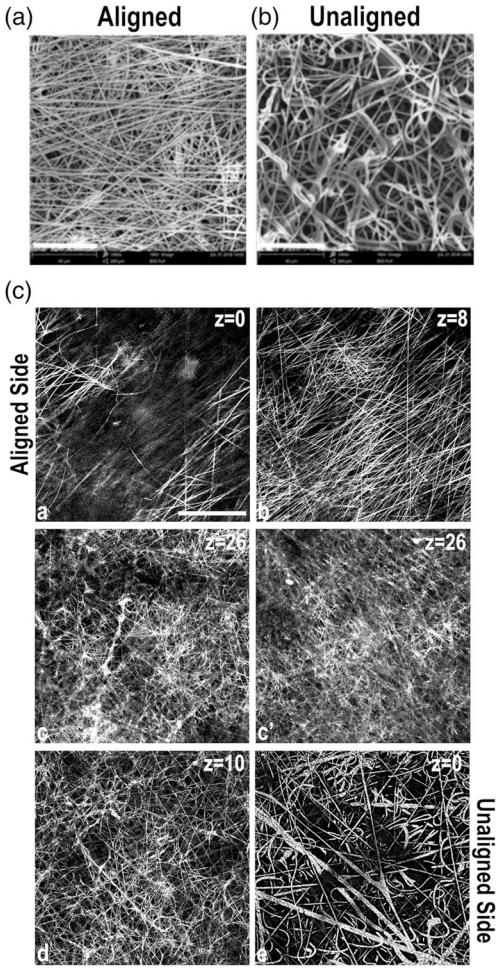

FIGURE 1.

Fiber orientations in a multilayered electrospun scaffold. Representative scanning electron microscope (SEM) images of the aligned (a) and unaligned (b) sides of the E1001(1k) scaffold are shown. Scale bar = 80 μm. (c) Confocal microscopy images were collected in reflectance mode to capture the structure of the scaffold fibers. Then, 2 μm thick confocal slices are shown starting from aligned (images a–c) and unaligned (images c′–e) sides. z corresponds to the distance from the scaffold surface. Images are representative of scaffold structure. Scale bar = 50 μm

Author Manuscript Author Manuscript Author Manuscript Author Manuscript

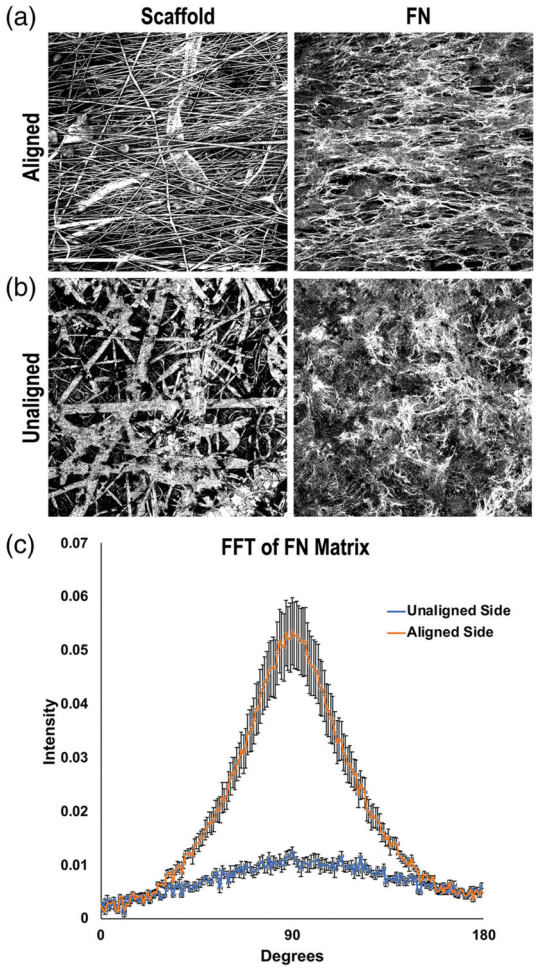

FIGURE 2.

Fibronectin (FN) matrix fibril orientations on the electrospun scaffold. Mouse NIH 3T3 fibroblasts were seeded onto either the aligned (a) or unaligned (b) side of separate scaffolds and grown for 7 days. Cells were fixed and stained with R457 anti-FN antiserum. Representative reflectance (scaffold) and FN confocal images of the same fields of view are shown. Scale bar = 50 μm. (c) FN fibril orientations on either side of the scaffold were quantified by fast Fourier transform (FFT) analysis of fluorescent images. Five images were averaged per condition and radial intensity data were plotted from 0 to 180° (error bars = *SEM*)

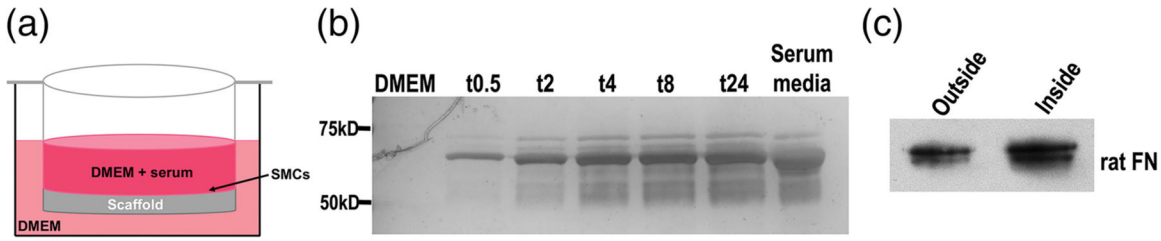

FIGURE 3.

Assessment of scaffold permeability. (a) Schematic of the transwell design showing confluent smooth muscle cell (SMCs) in Dulbecco's modified Eagle's media (DMEM) + serum on the scaffold surface inside the transwell and DMEM without serum on the outside of the transwell. (b) Aliquots of medium were collected from the outside of the transwell at the indicated times in hours. Equal volumes of medium were separated on an 8% polyacrylamide-SDS gel and proteins were detected by silver staining. DMEM alone and serum-containing medium were used as negative and positive controls, respectively. Molecular mass standards are shown on the left. (c) SMCs were cultured on a transwell scaffold for 5 days and then aliquots of media were collected from both sides of the transwell and immunoblotted with IC3 anti-FN monoclonal antibody

Author Manuscript Author Manuscript Author Manuscript Author Manuscript

Author Manuscript Author Manuscript Author Manuscript Author Manuscript

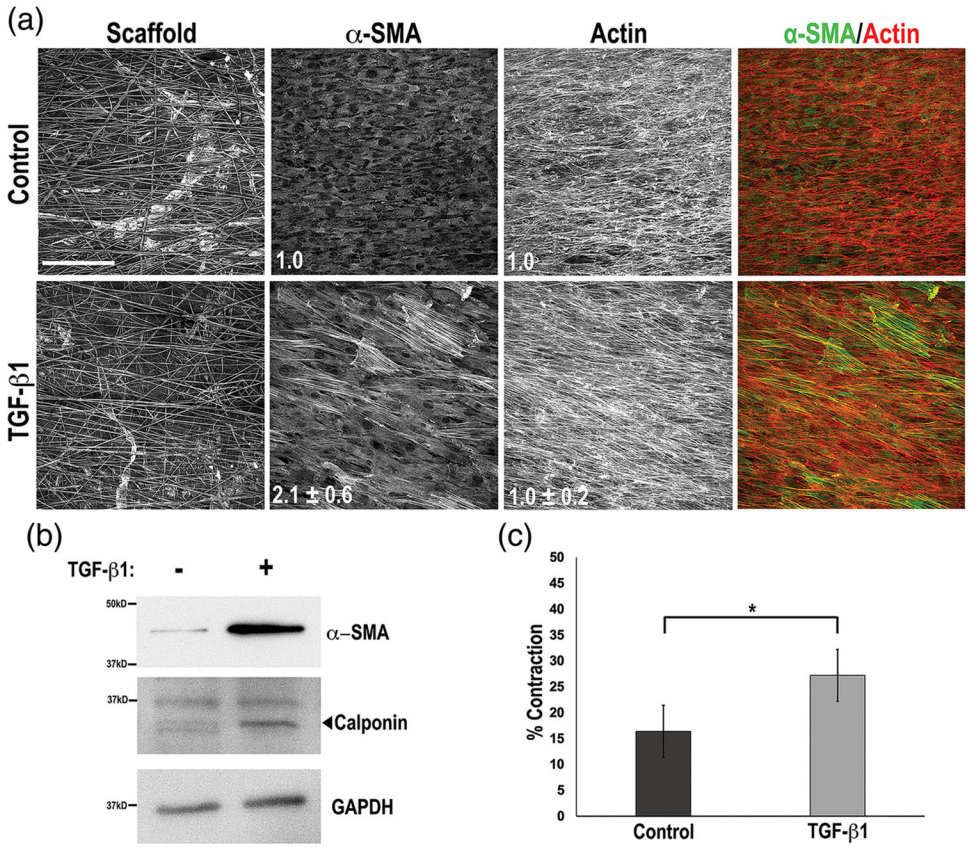

FIGURE 4.

Development of smooth muscle cell (SMC) contractile phenotype. (a) WKY3M22 rat SMCs on the aligned side of the multilayered scaffold at confluence were incubated in medium with either 2 ng/ml transforming growth factor-beta 1 (TGF-β1) (bottom) or vehicle (top) for days. Cells were fixed and stained with anti-alpha smooth muscle actin (α-SMA) antibody (green) and Texas-Red phalloidin to detect actin (red). The fold change in mean fluorescence intensities of TGF-β1-treated samples compared to control are shown in white (mean ± *SE*) for both α-SMA and actin ($n = 3$). (b) Cells grown and treated as in A were lysed in RIPA buffer. Samples were separated on a 10% polyacrylamide-SDS gel followed by immunoblotting with anti-α-SMA, anti-calponin, or anti-GAPDH antibodies. Representative blots are shown. (c) Contraction of fibrin-FN matrices containing TGF-β1-treated or control WKY3M22 SMCs was measured at 4 hr of incubation. Percent contraction was calculated and the data are expressed as mean ± *SE* for three experiments. $*p < .05$

Author Manuscript Author Manuscript Author Manuscript Author Manuscript

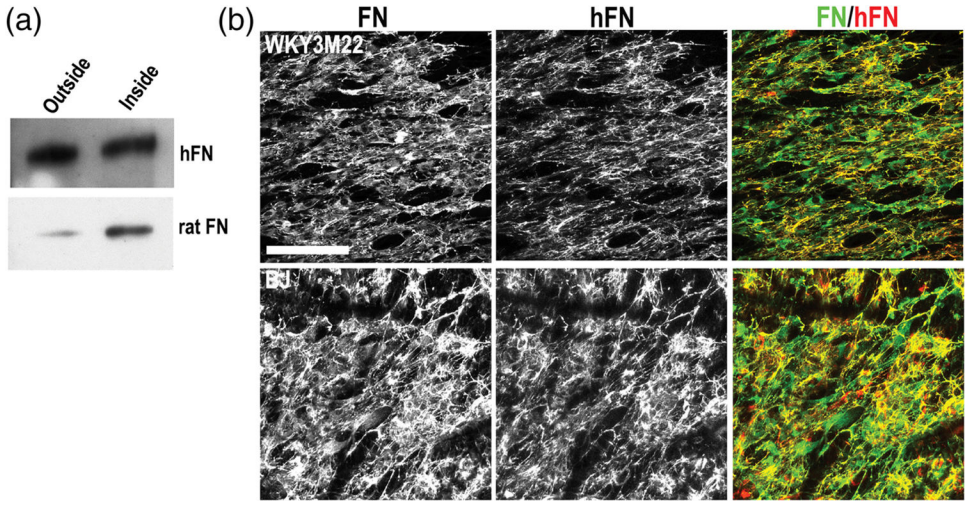

FIGURE 5.

Fibronectin (FN) transit and matrix assembly in a smooth muscle cell (SMC)-fibroblast scaffold coculture. (a) Fibroblasts and SMCs were cultured on opposite sides of a transwell scaffold for 5 days. Conditioned medium was collected from each side and FN was isolated by gelatin-Sepharose pulldown. FN was separated on an 8% polyacrylamide-SDS gel and immunoblotted with antibodies specific to either human FN (top) or rat FN (bottom). (b) BJ human fibroblasts and WKY3M22 rat SMCs were grown to confluence on unaligned and aligned sides of the scaffold, respectively. After 5 days, samples were fixed and stained with R457 anti-fibronectin antiserum to detect total FN (green) or HFN7.1 anti-human FN antibody (red). Representative images are shown. Scale bar = 50 μm

Author Manuscript Author Manuscript Author Manuscript Author Manuscript

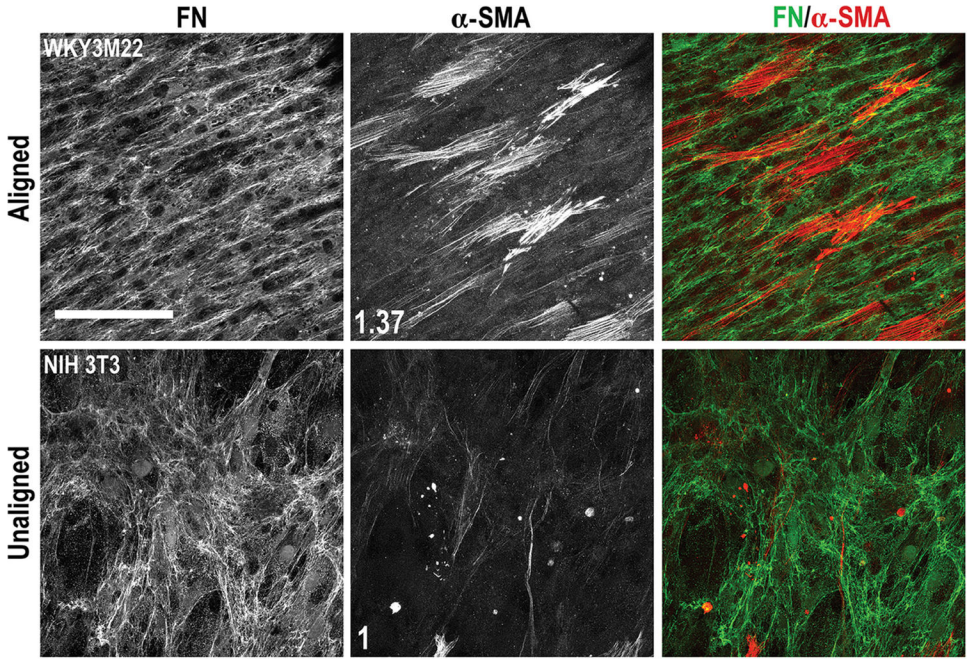

FIGURE 6.

Effects of transforming growth factor-beta 1 (TGF-β1) in a scaffold coculture of smooth muscle cells (SMCs) and fibroblasts. WKY3M22 SMCs (top panels) and NIH 3T3 fibroblasts (bottom panels) were grown to confluence on the aligned and unaligned sides of the scaffold, respectively. TGF-β1 was then added to the medium and the coculture was incubated for 3 days. Cells were fixed and stained with R457 antiserum for FN (green) and with anti-alpha smooth muscle actin (α-SMA) antibody (red). The fold changes in mean fluorescence intensity of SMCs compared to fibroblasts are shown in white (average of 6–8 fields of view). Scale bar = 50 μm

Author Manuscript Author Manuscript Author Manuscript Author Manuscript

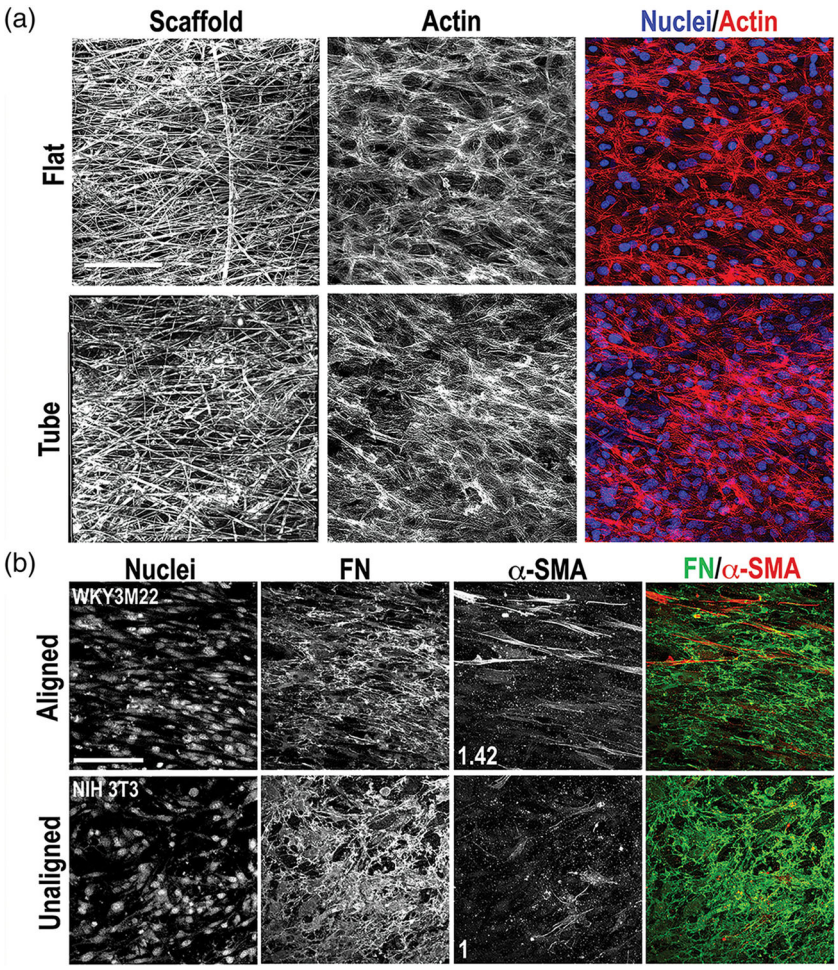

FIGURE 7.

Cell and matrix organization in a tubular scaffold. (a) Growth and alignment of WKY3M22 smooth muscle cells (SMCs) was compared on flat and tubular scaffolds. Cells were seeded onto the aligned side of two flat scaffold sheets. One sheet was rolled into a tube with the aligned fibers oriented circumferentially. After 7 days of culture, cells on both formats were fixed and stained with Texas Red-Phalloidin and DAPI to detect actin (red) and nuclei (blue), respectively. Representative images are shown. (b) WKY3M22 SMCs and NIH 3T3 cells were seeded on opposite sides of a scaffold as in Figure 6 and a cell-scaffold construct was rolled into a tube as in (a). Materials were fixed and stained after 5 days in culture using antibodies against FN (green) and alpha smooth muscle actin (α-SMA) (red). The fold change in mean fluorescence intensity of SMCs compared to fibroblasts are shown in white (average of 6–8 fields of view). Scale bars = 50 μm